JACS
JOURNAL OF THE AMERICAN CHEMICAL SOCIETY
Communication
pubs.acs.org/JACS

# DNA Aptamer-Based Activatable Probes for Photoacoustic Imaging in Living Mice

Jingjing Zhang,[†,‡,§] Lukas P. Smaga,[†,‡,§] Nitya Sai Reddy Satyavolu,[†,‡] Jefferson Chan,[*,†,‡] and Yi Lu[*,†,‡]

[†]Department of Chemistry, [‡]Beckman Institute for Advanced Science and Technology, University of Illinois at Urbana−Champaign, Urbana Illinois 61801, United States

Supporting Information

**ABSTRACT:** DNA aptamers are a powerful class of molecules for sensing targets, but have been limited when applied to imaging in living animals because most aptamer probes are fluorescence-based, which limits imaging penetration depth. Photoacoustic (PA) imaging emerged as an alternative to MRI and X-ray tomography in biomedical imaging, due to its ability to afford high-resolution images at depths in the cm range. Despite its promise, PA imaging is limited by a lack of strategies to design selective and activatable probes for targets. To overcome this limitation, we report design and demonstration of PA probes based on DNA aptamers that can hybridize to DNA strands conjugated to a near-infrared fluorophore/quencher pair (IRDye 800CW/IRDye QC-1) with efficient contact quenching. Binding of the target triggered a release of the DNA strand with the quencher and thus relief of the contact quenching, resulting in a change of the PA signal ratio at 780/725 nm. Using thrombin as a model, a relationship was established between the thrombin concentrations and the PA ratio, with a dynamic range of 0−1000 nM and a limit of detection of 112 nM. Finally, *in vivo* PA imaging studies showed that the PA ratio increased significantly 45 min after injection of thrombin but not with injection of PBS as a vehicle control, demonstrating the first aptamer-based activatable PA probe for advanced molecular imaging in living mice. Since *in vitro* selection can obtain aptamers selective for many targets, the design demonstrated can be applied for PA imaging of a number of targets.

DNA aptamers are a powerful class of recognition agents for sensing and imaging targets,[1] ranging from small organic metabolites to biomolecules, to viruses[2] or cells,[3] because aptamers for recognizing almost any target can be obtained using a combinatorial method called SELEX.[4] Hence, many aptamers have been converted into fluorescent,[5] colorimetric[6] and electronical sensors.[7] Among them, fluorescent sensors remain dominant probes for biomedical applications,[5a−e,8] because of their high intensity and fast signal response. Despite progress, most fluorescent probes lack penetration depth necessary for *in vivo* applications such as imaging in live mice.[9]

Photoacoustic (PA) imaging is a promising method for medical diagnostics and imaging,[10] because it integrates optical excitation with ultrasonic detection based on the PA effect; in comparison with fluorescent imaging, the penetration depth of PA imaging is greater (cm vs mm),[9b,11] making it possible to image deep tissues with high resolution. To visualize physiological and pathological targets at the molecular level, most PA imaging methods utilizes endogenous or exogenous light absorbers as entities to provide the optical contrast in biological tissues.[12] Though most PA probes produce signals through accumulation in the targeted tissue,[13] it is difficult to quantify local concentrations of the target, because these probes typically do not change their signals upon interaction with the target of interest. To overcome this limitation, activatable PA probes that combine molecular recognition with a modulation of the PA signal (e.g., by a shift in the absorbance peak upon binding of their target) have been developed.[14] Despite progress, these activatable PA probes are only available for a limited number of targets, such as enzymes,[14c,e,15] pH/temperature,[16] metal ions,[12d] and small molecule mediators,[12b] probably due to their complex design and synthesis. To reach the full potential of PA imaging, there is a need for more strategies in the design of PA probes that can be applied to a range of targets, while maintaining advantages of easy synthesis and functionalization.

The challenge for the development of activatable DNA-based PA probes lies in the creation of substantial and specific absorption changes in the near-infrared (NIR) region upon activation by the target, because PA signals are correlated with absorption. To meet this challenge, we report a strategy for the design of activatable PA probes based on DNA aptamers that can hybridize to DNA strands conjugated to a NIR fluorophore/quencher pair with efficient contact quenching. Assembly and disassembly of the DNA complex could either trigger or inhibit the quenching reaction, resulting in a change of the PA signal at two maximum absorption wavelengths. Using this probe, thrombin, our model target, was detected through PA imaging.

We chose IRDye 800CW as the fluorophore due to its high absorption in the NIR region and IRDye QC-1 as the NIR dark quencher (Figure S1). Fluorescent detection occurs generally by one of two mechanisms: FRET or contact quenching. Though FRET does not affect the probe's absorption spectrum, contact quenching often causes distinct changes in the absorption spectrum due to coupling of the excited-state energy levels.[17] Since energy transfer in a contact mode is related to substantial absorption changes, we hypothesized that such a quenching system might also possess the ability to produce a detectable PA

**Received:** July 27, 2017
**Published:** October 13, 2017




DOI: 10.1021/jacs.7b07913
J. Am. Chem. Soc. 2017, 139, 17225−17228

signal in response to the target, without the need of complex design and synthesis for signal transduction.

In designing our functional DNA-based PA probe, we took advantage of the unique optical properties of these two species (Scheme 1). In the intact state, DNAs labeled with IRDye

**Scheme 1. Proposed Mechanism for Ratiometric Photoacoustic Imaging Based on Functional DNA Probes**

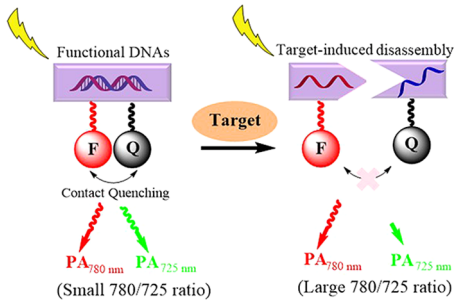


800CW and IRDye QC-1 were assembled, bringing the two moieties into close proximity (e.g., <20 Å).[18] The formation of the DNA complex would allow interaction between the two dyes, resulting in a contact-mediated quenching. PA signals produced at these two wavelengths ($PA_1$ and $PA_2$) correspond to the absorption maxima of the two moieties within the probe. In the presence of the target, the contact-mediated quenching could be inhibited through target-induced disassembly of the DNA complex, resulting in distinct changes of the PA signal at the above two wavelengths. Therefore, the ratio of PA signals is expected to change in response to the target. Based on this general strategy, the development of activatable PA probes for imaging and quantification of various targets will be possible.

To demonstrate the design, we chose an aptamer as the recognition unit[19] and thrombin, a trypsin-like serine proteinase that plays a major role in blood coagulation,[20] as the target. As shown in Figure 1a, the thrombin binding aptamer (TBA) forms a DNA duplex structure through hybridizing with IRDye 800CW-labeled single stranded (ss) DNA (FDNA) and IRDye QC-1 quencher-labeled ssDNA (QDNA). In absence of thrombin, hybridization places IRDye next to its quencher, causing both fluorescent and PA signals to be low. In presence of thrombin, binding of the target by TBA weakens the hybridization between TBA-QDNA, causing a release of FDNA from the duplex and thus an increase of fluorescent and PA signals. This assembly and disassembly process was first verified by fluorescence spectroscopy. As shown in Figure S2, the spectrum of FDNA displayed a distinct fluorescent signal with a maximum emission at 797 nm when the sample was excited at 764 nm. This emission is derived from IRDye 800CW. Upon addition of TBA and QDNA, the fluorescent signal showed a major decrease, probably due to formation of the duplex shown in Figure 1a and the resulting contact-mediated quenching. Addition of 1000 nM thrombin restored fluorescent signal intensity, likely a result of binding of thrombin that caused dehybridization of the QDNA away from the duplex.

To corroborate the result from the fluorescent study, we used UV−vis spectroscopy. As shown in Figure 1b, both FDNA and QDNA by themselves showed a distinct absorption in the NIR range, with maximum absorption wavelengths at 780 and 825 nm, respectively. Upon the addition of TBA, a new absorption band centered at 725 nm emerged, whereas the above two absorption bands remained with slight change of intensity. This result indicated the thrombin aptamer could cause assembly of the two labeled DNAs, and bring the fluorophore/quencher pair close to each other, resulting in strong contact quenching. Upon addition of thrombin, the absorbance at 725 nm showed a distinct decrease, whereas the absorbance at 780 nm displayed a small increase (Figure 1b). These results indicated addition of thrombin could induce the disassembly of the DNA probe, inhibiting the contact quenching. Therefore, upon laser irradiation, the DNA duplex structure should produce three distinct PA signals at 725, 780 and 825 nm (Figure S3). $PA_{725}$ is mainly due to the contribution from contact quenching, whereas $PA_{780}$ could be due to contributions from both IR800 dye and the quencher, due to their spectral overlap around 780 nm, shown in the UV−vis spectra of DNA probe and its building blocks (Figure 1b). However, $PA_{825}$, mainly due to contributions from

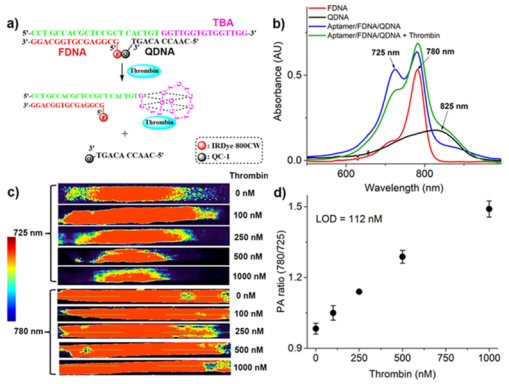


**Figure 1.** (a) Scheme of structure-switching DNA aptamer complex for ratiometric photoacoustic imaging of thrombin. (b) UV−vis absorption spectra of the aptamer complex in response to thrombin. (c) Photoacoustic imaging of thrombin with different concentrations. Color code: low intensity blue, high intensity red. (d) The PA signal ratios at 780/725 nm in response to thrombin.

the quencher, is much smaller than the signals at 725 and 780 nm. To achieve optimal performance of the probe, the two highest absorption peaks at 725 and 780 nm were chosen as the excitation wavelengths for our PA imaging experiments. To further investigate the change of PA signals after disassembly of the probe, we induced disassembly by using a partially complementary DNA strand (cDNA) of TBA (Figure S4a). In absence of cDNA, two strong PA signals were obtained at both 725 and 780 nm. In contrast, under the same conditions, addition of cDNA resulted in a decrease of $PA_{725}$, whereas $PA_{780}$ exhibited minimal change (Figure S4b). As the cDNA concentration increases, the $PA_{780}/PA_{725}$ ratio increases significantly (Figure S4c). The difference between the two positive groups and the control group is significant ($p < 0.05$). The decrease of $PA_{725}$ was due to the disassembly of DNA probe by cDNA, which inhibited contact quenching. The small change in $PA_{780}$ may be due to compensatory effects through absorbance, fluorescence and other processes that contribute to and affect the PA signal of the probe at 780 nm.[14c]

Figure 1c shows PA images of thrombin at different concentrations using the DNA probe designed in Figure 1a. In the absence of thrombin, two strong PA signals were obtained at 725 and 780 nm. In contrast, under the same conditions, addition of thrombin resulted in a decrease of $PA_{725}$, whereas $PA_{780}$ exhibited minimal change (Figure 1c). This observation is consistent with the fluorescence and UV−vis spectroscopic results, which indicated that addition of thrombin caused


DOI: 10.1021/jacs.7b07913
J. Am. Chem. Soc. 2017, 139, 17225−17228

disassembly of the DNA duplex structure, leading to an inhibition of the contact-mediated quenching between the fluorophore and its quencher. Using the PA signal ratio between 780 and 725 nm as a measure, we observed a quantitative relationship between $PA_{780}/PA_{725}$ and the thrombin concentration in HEPES buffer in the range of 0−1000 nM, with a limit of detection (LOD) of 112 nM (based on $3\sigma_b$/slope, where $\sigma_b$ is the standard deviation of the blank samples).

To demonstrate selectivity of the DNA probe, we carried out a control experiment with three common proteins (BSA, streptavidin, cytochrome c), which had no interaction with the thrombin aptamer.[21] As shown in Figure S5, normalized $PA_{780}/PA_{725}$ obtained with these three competing proteins did not show a significant difference in comparison with the buffer ($p > 0.05$). In contrast, the normalized $PA_{780}/PA_{725}$ in response of thrombin was significantly higher ($p < 0.05$). In addition, the detection of thrombin in presence of a mixture of the above three proteins was also evaluated (Figure S5b), and no significant difference was observed in comparison with the thrombin detection in buffer ($p > 0.05$). These results indicate that the probe retains its analyte selectivity in more complex matrices.

To explore whether the PA probe can be applied in biological samples, we first tested it in human serum. As shown in Figure 2,

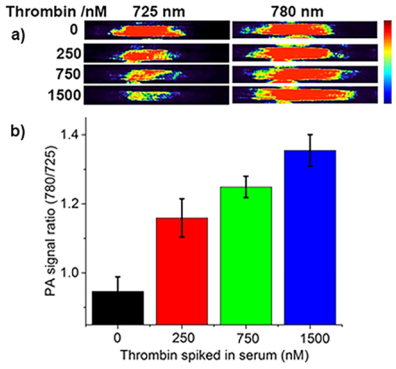


**Figure 2.** (a) PA imaging of thrombin spiked in serum using our DNA probe. Color code: low intensity blue, high intensity red. (b) PA signal ratio (780/725 nm) of the probe in response to thrombin.

$PA_{725}$ decreased with increasing concentrations of thrombin added, whereas $PA_{780}$ exhibited minimal change. In addition, we observed a quantitative relationship between $PA_{780}/PA_{725}$ and the thrombin spiked in human serum in the range of 0−1500 nM, with a LOD of 344 nM based on $3\sigma_b$/slope. Since these results are similar to those in buffer, they suggest other components in the serum did not interfere significantly with the probe performance, and therefore this PA probe can be used in complex body fluids.

Finally, to test the feasibility of the DNA probe for *in vivo* PA imaging of thrombin, the DNA probe was subcutaneously injected into the flanks of BALB/c mice, followed by injection of thrombin and PBS (vehicle control) to the left and right flanks, respectively (Figure 3a). At 45 min after the injection, PA images were recorded at 725 and 780 nm. As shown in Figure 3b,c, mice showed intrinsically weak background signals, which probably derive from the absorption of oxy- and deoxyhemoglobin,[22] whereas both $PA_{725}$ and $PA_{780}$ increased significantly after injection of the DNA probe, indicating good PA properties of the DNA probe. Furthermore, 45 min after the injection, thrombin-treated mice (Figure 3c) showed a much weaker signal at $PA_{725}$ compared with the PBS-treated control mice (Figure 3b),

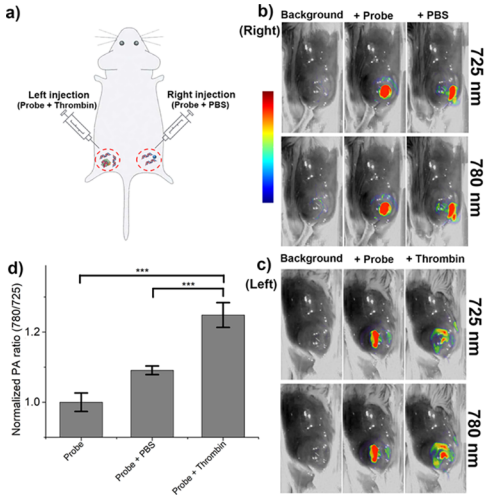


**Figure 3.** *In vivo* PA imaging of thrombin. (a) PA images from left flank (thrombin injection) and right flank (PBS injection), respectively. Representative PA images of mice before and after subcutaneous injection of DNA probes with PBS (b) and thrombin (c). Color code: low intensity blue, high intensity red. (d) Normalized PA signal ratio at 780/725 nm before and 45 min after injection of PBS or thrombin. Error bars represent standard deviations of three separate measurements ($n = 3$). Asterisks indicate significant differences ($p < 0.001$).

indicating disassembly of the DNA probe via activation through thrombin but not PBS. To measure changes of $PA_{725}$ and $PA_{780}$ in response to PBS and thrombin, we subtracted the PA signals of $PA_{725}$ from $PA_{780}$ on right and left flanks, respectively. As shown in Figure S3, the difference between $PA_{725}$ and $PA_{780}$ changed in the thrombin group, indicating a ratiometric turn-on response to thrombin upon the normalization of the two PA ratios. We further tested the time dependence of the change of the normalized $PA_{780}/PA_{725}$ in response to PBS and thrombin. As shown in Figure S6, for 30 min after the injection, there is no significant difference of normalized $PA_{780}/PA_{725}$ in PBS-treated mice ($p > 0.05$), whereas a significant higher $PA_{780}/PA_{725}$ was observed in the thrombin-treated mice ($p < 0.05$). When the time increased from 30 to 45 min after injection, the PA signal ratio at the control flank (PBS) increased; however, the ratio increase at the thrombin-treated flanks was significantly higher (Figure S6b). Therefore, we chose 45 min as optimal imaging time. These results indicated our DNA probe retained the aptamer functionality that could selectively recognize thrombin in a living system. As shown in Figure 3d, thrombin-treated mice had a higher $PA_{780}/PA_{725}$ ratio than both untreated and PBS treated mice. The difference between the positive group and the two control groups is significant ($p < 0.001$), which is compatible to that of thrombin imaging using thrombin-activatable peptides.[23] These results demonstrate that our DNA probe can be activated by exogenously added thrombin in living mice, indicating its great potential for advanced molecular imaging *in vivo*.

In summary, we demonstrated the design and evaluation of a DNA aptamer-based PA probe that provides a target-dependent PA signal change, enabling selective visualization and quantification of the targets that the aptamer recognizes. The sensor system is based on the contact quenching between the NIR dye (IRDye 800CW) and its dark quencher (IRDye QC-1), brought together through DNA aptamer mediated duplex formation. Assembly and disassembly of the DNA complex could either trigger or inhibit the contact quenching, resulting in a change of the PA signal at its two maximum absorption wavelengths. Using


DOI: 10.1021/jacs.7b07913
J. Am. Chem. Soc. 2017, 139, 17225−17228

this approach, thrombin has been detected in both buffer and human serum through PA imaging. Finally, the aptamer-based PA probe exhibited an enhanced and specific ratiometric change in PA signals toward thrombin injection *in vivo*, demonstrating the first aptamer-based activatable PA probe for advanced molecular imaging in living mice. As many DNA aptamers have been obtained for selective binding of a broad range of targets, the design demonstrated will provide an approach for quantitative detection and imaging of a wide range of targets. Additionally, the proposed PA imaging approach via target-induced DNA disassembly should be applicable for the *in vivo* imaging of overexpressed miRNAs in cancerous tissues using suitable functional-DNA partners.

## ■ ASSOCIATED CONTENT

### Supporting Information

The Supporting Information is available free of charge on the ACS Publications website at DOI: 10.1021/jacs.7b07913.

Experimental details and characterization data (PDF)

## ■ AUTHOR INFORMATION


### Corresponding Authors

*yi-lu@illinois.edu

*jeffchan@illinois.edu

### ORCID

Jefferson Chan: 0000-0003-4139-4379

Yi Lu: 0000-0003-1221-6709

### Author Contributions

§These authors contributed equally.


### Notes

The authors declare no competing financial interest.

## ■ ACKNOWLEDGMENTS

We thank the U.S. National Institutes of Health (GM124316 and MH110975) for financial support. N. S. R. S. would like to thank the Beckman Graduate Fellowship for financial support.

## ■ REFERENCES


(1) (a) Kuai, H.; Zhao, Z.; Mo, L.; Liu, H.; Hu, X.; et al. *J. Am. Chem. Soc.* **2017**, *139*, 9128. (b) Wan, S.; Zhang, L.; Wang, S.; Liu, Y.; Wu, C.; et al. *J. Am. Chem. Soc.* **2017**, *139*, 5289. (c) Famulok, M.; Mayer, G. *Acc. Chem. Res.* **2011**, *44*, 1349. (d) Li, D.; Song, S. P.; Fan, C. H. *Acc. Chem. Res.* **2010**, *43*, 631. (e) Lan, L.; Yao, Y.; Ping, J.; Ying, Y. *ACS Appl. Mater. Interfaces* **2017**, *9*, 23287. (f) Lao, Y. H.; Phua, K. K.; Leong, K. W. *ACS Nano* **2015**, *9*, 2235. (g) Iliuk, A. B.; Hu, L.; Tao, W. A. *Anal. Chem.* **2011**, *83*, 4440. (h) Zhou, W.; Saran, R.; Liu, J. *Chem. Rev.* **2017**, *117*, 8272. (i) Du, Y.; Li, B.; Wang, E. *Acc. Chem. Res.* **2013**, *46*, 203. (j) Ye, D. K.; Zuo, X. L.; Fan, C. H. *Prog. Chem.* **2017**, *29*, 36.

(2) (a) Labib, M.; Zamay, A. S.; Muharemagic, D.; Chechik, A. V.; Bell, J. C.; et al. *Anal. Chem.* **2012**, *84*, 1813. (b) Bai, W.; Spivak, D. A. *Angew. Chem., Int. Ed.* **2014**, *53*, 2095.

(3) (a) Liang, H.; Zhang, X. B.; Lv, Y. F.; Gong, L.; Wang, R. W.; et al. *Acc. Chem. Res.* **2014**, *47*, 1891. (b) Li, L.-L.; Wu, P.; Hwang, K.; Lu, Y. *J. Am. Chem. Soc.* **2013**, *135*, 2411. (c) Xing, H.; Hwang, K.; Li, J.; Torabi, S.-F.; et al. *Curr. Opin. Chem. Eng.* **2014**, *4*, 79.

(4) (a) Zhang, L. Q.; Wan, S.; Jiang, Y.; Wang, Y. Y.; et al. *J. Am. Chem. Soc.* **2017**, *139*, 2532. (b) Li, X. L.; An, Y.; Jin, J.; Zhu, Z.; Hao, L. L.; et al. *Anal. Chem.* **2015**, *87*, 4941. (c) Nutiu, R.; Li, Y. F. *Angew. Chem., Int. Ed.* **2005**, *44*, 1061. (d) Gotrik, M. R.; Feagin, T. A.; Csordas, A. T.; Nakamoto, M. A.; Soh, H. T. *Acc. Chem. Res.* **2016**, *49*, 1903. (e) Liu, J. W.; Cao, Z. H.; Lu, Y. *Chem. Rev.* **2009**, *109*, 1948. (f) Liu, J.; Lu, Y. *Nat. Protoc.* **2006**, *1*, 246. (g) Gu, C.; Lan, T.; Shi, H.; Lu, Y. *Anal. Chem.* **2015**, *87*, 7676.

(5) (a) Liu, X. Q.; Wang, F.; Aizen, R.; Yehezkeli, O.; Willner, I. *J. Am. Chem. Soc.* **2013**, *135*, 11832. (b) Chen, T. T.; Tian, X.; Liu, C. L.; Ge, J.; Chu, X.; et al. *J. Am. Chem. Soc.* **2015**, *137*, 982. (c) Liu, Z. B.; Chen, S. S.; Liu, B. W.; Wu, J. P.; Zhou, Y. B.; et al. *Anal. Chem.* **2014**, *86*, 12229. (d) Wang, L.; Zhu, J. B.; Han, L.; Jin, L. H.; Zhu, C. Z.; et al. *ACS Nano* **2012**, *6*, 6659. (e) Li, J. J.; Zhong, X. Q.; Zhang, H. Q.; Le, X. C.; Zhu, J. J. *Anal. Chem.* **2012**, *84*, 5170. (f) Qu, X. M.; Zhu, D.; Yao, G. B.; Su, S.; Chao, J.; et al. *Angew. Chem., Int. Ed.* **2017**, *56*, 1855. (g) Liu, J.; Lee, J. H.; Lu, Y. *Anal. Chem.* **2007**, *79*, 4120.

(6) (a) Golub, E.; Albada, H. B.; Liao, W. C.; Biniuri, Y.; Willner, I. *J. Am. Chem. Soc.* **2016**, *138*, 164. (b) Xia, F.; Zuo, X. L.; Yang, R. Q.; Xiao, Y.; Kang, D.; et al. *Proc. Natl. Acad. Sci. U. S. A.* **2010**, *107*, 10837. (c) Rana, M.; Balcioglu, M.; Robertson, N. M.; Hizir, M. S.; Yumak, S.; et al. *Chem. Sci.* **2017**, *8*, 1200.

(7) (a) Li, H.; Arroyo-Curras, N.; Kang, D.; Ricci, F.; Plaxco, K. W. *J. Am. Chem. Soc.* **2016**, *138*, 15809. (b) Yang, J. M.; Dou, B. T.; Yuan, R.; Xiang, Y. *Anal. Chem.* **2017**, *89*, 5138. (c) Mahshid, S. S.; Ricci, F.; Kelley, S. O.; Vallee-Belisle, A. *ACS Sens.* **2017**, *2*, 718.

(8) (a) Li, J. J.; Cheng, F. F.; Huang, H. P.; Li, L. L.; Zhu, J. J. *Chem. Soc. Rev.* **2015**, *44*, 7855. (b) Hong, G.; Antaris, A. L.; Dai, H. *Nat. Biomed. Eng.* **2017**, *1*, 0010.

(9) (a) Ntziachristos, V. *Nat. Methods* **2010**, *7*, 603. (b) Kim, C.; Favazza, C.; Wang, L. H. V. *Chem. Rev.* **2010**, *110*, 2756. (c) Sanderson, M. J.; Smith, I.; Parker, I.; Bootman, M. D. *Cold Spring Harb. Protoc.* **2014**, *2014*, DOI: 10.1101/pdb.top071795.

(10) (a) Wang, L. H. V.; Hu, S. *Science* **2012**, *335*, 1458. (b) Li, S.; Chen, Y.; Liu, H.; Wang, Y.; Liu, L.; et al. *Chem. Mater.* **2017**, *29*, 6087.

(11) Xia, J.; Yao, J. J.; Wang, L. V. *Prog. Electromagn. Res.* **2014**, *147*, 1.

(12) (a) Huang, P.; Rong, P. F.; Lin, J.; Li, W. W.; Yan, X. F.; et al. *J. Am. Chem. Soc.* **2014**, *136*, 8307. (b) Pu, K.; Shuhendler, A. J.; Jokerst, J. V.; Mei, J.; Gambhir, S. S.; et al. *Nat. Nanotechnol.* **2014**, *9*, 233. (c) Dogra, V.; Chinni, B.; Singh, S.; Schmitthenner, H.; Rao, N.; et al. *J. Biomed. Opt.* **2016**, *21*, 66019. (d) Cash, K. J.; Li, C. Y.; Xia, J.; Wang, L. H. V.; Clark, H. A. *ACS Nano* **2015**, *9*, 1692.

(13) Weber, J.; Beard, P. C.; Bohndiek, S. E. *Nat. Methods* **2016**, *13*, 639.

(14) (a) Lyu, Y.; Zhen, X.; Miao, Y. S.; Pu, K. Y. *ACS Nano* **2017**, *11*, 358. (b) Miao, Q. Q.; Pu, K. Y. *Bioconjugate Chem.* **2016**, *27*, 2808. (c) Levi, J.; Kothapalli, S. R.; Ma, T. J.; Hartman, K.; Khuri-Yakub, B. T.; et al. *J. Am. Chem. Soc.* **2010**, *132*, 11264. (d) Li, H.; Zhang, P.; Smaga, L. P.; Hoffman, R. A.; Chan, J. *J. Am. Chem. Soc.* **2015**, *137*, 15628. (e) Dragulescu-Andrasi, A.; Kothapalli, S. R.; Tikhomirov, G. A.; Rao, J. H.; Gambhir, S. S. *J. Am. Chem. Soc.* **2013**, *135*, 11015. (f) Ng, K. K.; Shakiba, M.; Huynh, E.; Weersink, R. A.; Roxin, A.; et al. *ACS Nano* **2014**, *8*, 8363.

(15) Morgounova, E.; Shao, Q.; Hackel, B. J.; Thomas, D. D.; Ashkenazi, S. *J. Biomed. Opt.* **2013**, *18*, 56004.

(16) Chen, Q.; Liu, X. D.; Chen, J. W.; Zeng, J. F.; Cheng, Z. P.; et al. *Adv. Mater.* **2015**, *27*, 6820.

(17) Johansson, M. K.; Fidder, H.; Dick, D.; Cook, R. M. *J. Am. Chem. Soc.* **2002**, *124*, 6950.

(18) Simard, B.; Tomanek, B.; van Veggel, F. C. J. M.; Abulrob, A. *Photoch. Photobio. Sci.* **2013**, *12*, 1824.

(19) Nutiu, R.; Li, Y. F. *J. Am. Chem. Soc.* **2003**, *125*, 4771.

(20) Wang, J.; Wei, Y. R.; Hu, X. X.; Fang, Y. Y.; Li, X. Y.; et al. *J. Am. Chem. Soc.* **2015**, *137*, 10576.

(21) Yigit, M. V.; Mazumdar, D.; Lu, Y. *Bioconjugate Chem.* **2008**, *19*, 412.

(22) Yin, C.; Zhen, X.; Fan, Q. L.; Huang, W.; Pu, K. Y. *ACS Nano* **2017**, *11*, 4174.

(23) (a) Jaffer, F. A.; Tung, C. H.; Gerszten, R. E.; Weissleder, R. *Arterioscler., Thromb., Vasc. Biol.* **2002**, *22*, 1929. (b) Whitney, M.; Savariar, E. N.; Friedman, B.; Levin, R. A.; Crisp, J. L.; et al. *Angew. Chem., Int. Ed.* **2013**, *52*, 325.